2013

Porous titania nanosheet/nanoparticle hybrids as photoanodes for dye-sensitized solar cells

Yang Bai
University of Queensland

Zheng Xing
University of Queensland

Hua Yu
University of Queensland

Zhen Li
University of Wollongong, zhenl@uow.edu.au

Rose Amal
University of New South Wales, r.amal@unsw.edu.au

See next page for additional authors

Porous titania nanosheet/nanoparticle hybrids as photoanodes for dye-sensitized solar cells

Abstract

Porous titania nanohybrids (NHs) were successfully prepared by hybridizing the exfoliated titania nanosheets with anatase TiO2 nanoparticles. Various characterizations revealed that the titania NHs as photoanodes play a trifunctional role (light harvesting, dye adsorption, and electron transfer) in improving the efficiency (η) of the dye-sensitized solar cells. The optimized photoanode consisting layered NHs demonstrated a high overall conversion efficiency of 10.1%, remarkably enhanced by 29.5% compared to that (7.8%) obtained from the benchmark P25 nanoparticles under the same testing conditions.

Keywords

sensitized, solar, cells, nanosheet, nanoparticle, porous, hybrids, titania, photoanodes, dye

Disciplines

Engineering | Physical Sciences and Mathematics

Publication Details

Bai, Y., Xing, Z., Yu, H., Li, Z., Amal, R. & Wang, L. (2013). Porous titania nanosheet/nanoparticle hybrids as photoanodes for dye-sensitized solar cells. ACS Applied Materials and Interfaces, 5 (22), 12058-12065.

Authors

Yang Bai, Zheng Xing, Hua Yu, Zhen Li, Rose Amal, and Lianzhou Wang

Porous Titania Nanosheet/Nanoparticle Hybrids as Photoanodes for Dye-sensitized Solar Cells

Yang Bai,[†] Zheng Xing,[†] Hua Yu,[†] Zhen Li,[‡] Rose Amal,[§] Lianzhou Wang*[†]

[†]ARC Centre of Excellence for Functional Nanomaterials, School of Chemical Engineering and Australian Institute for Bioengineering and Nanotechnology, The University of Queensland, Brisbane, QLD 4072 Australia.

[‡]Institute of Superconducting and Elctronic Materials, Australian Institute of Innovative Materials, The University of Wollongong, Northwollongong, NSW 2500, Australia.

[§]ARC Centre of Excellence for Functional Nanomaterials, School of Chemical Engineering, The University of New South Wales, Sydney, NSW 2052, Australia.

ABSTRACT: Porous titania nanohybrids (NHs) were successfully prepared by hybridizing the exfoliated titanate nanosheets with the anatase TiO_2 nanoparticles. Various characterizations revealed that the titania NHs as photoanodes play a tri-functional role (light harvesting, dye-adsorption and electron transfer) in improving the efficiency (η) of the DSSCs. The optimized photoanode consisting layered NHs demonstrated a high overall conversion efficiency of 10.1%, remarkably enhanced by 29.5% compared to that (7.8%) obtained from the benchmark P25 nanoparticles under the same testing conditions.

KEYWORDS: *exfoliated titania nanosheets, anatase nanoparticles, hybrid photoanodes, dye-sensitized solar cells*

INTRODUCTION

Inspired by the breakthrough work of M. Grätzel on dye-sensitized solar cells (DSSCs),[1] much effort has been made on tailoring photoanode architectures to improve the overall conversion efficiency in the past decades.[2-7] One of major drawbacks of the conventional TiO_2 nanoparticle photoanodes in DSSCs is the negligible light scattering of the films due to their small particle size ranging typically from *ca.* 20~30 nm, resulting in a low light harvesting efficiency. An optical scattering layer on top has been proposed as it could enhance the light harvest by localizing the incident light within the photoanode. So far, an array of light scattering materials has been investigated, including TiO_2 mesoporous microspheres,[7, 8] hollow spheres[9-11] and mirror-like nanoparticles.[12, 13]

Another major drawback of the conventional TiO_2 nanoparticle photoanodes is the low transport efficiency of electrons, which imposes an upper limit on the film thickness. In a film composed of TiO_2 nanoparticles, electrons diffuse to the surface of collector electrode (e.g. FTO substrate) through a zigzag pathway[14] and may easily recombine with the oxidizing species (predominately triiodide ions in the electrolyte), thus reducing the efficiency of DSSCs. Therefore, one-dimensional (1D) TiO_2[3, 15-17] and ZnO nanostructures,[5, 14, 18] and two-dimensional (2D) nanosheets[19, 20] have attracted recent attention in facilitating electron transport in DSSCs.

Even though the light harvesting and charge transfer efficiency can be enhanced by introducing an optical light scattering layer and fabrication of films from 1D and 2D nanostructures respectively, the surface area that is accessible to the dye is usually sacrificed, resulting in insufficient dye adsorption and thus limited conversion efficiency. Thereby how to efficiently transfer electrons and harvest light without compromise in dye adsorption, is believed to be one of the key challenges in achieving high-efficiency DSSCs.

Layered nanohybrids (NHs) by pillaring semiconducting nanoparticles such as CdS, α-Fe_2O_3, and TiO_2[21-24] into layered inorganic compounds[25-30] have recently drawn growing attention in photocatalysis, due to their large surface area as well as suppressed electron-hole recombination because of electron transfer between guest and host.[22, 23, 31] Titanate nanosheets ($Ti_{0.91}O_2$) derived from delamination of layered compounds have unique structural characteristic of ultimate two-dimensional anisotropy with extremely small thickness in the subnano- to nanometer scales, which leads to new physical and chemical properties for nanosheets.[32] In addition, the exfoliation of layered metal oxides into 2D nanosheets[33, 34] ($Ti_{0.91}O_2$ nanosheets) makes it possible to pillar large-sized (TiO_2) nanoparticles into the interlayer space of host materials through an exfoliation-restacking process of nanosheets and guest particles.[23, 35, 36] The obtained pillared NHs possesses highly controllable physical and chemical properties.[22, 37-39] In particular, due to the enlarged interlayer distance, the total surface area is significantly increased, facilitating chemical adsorption or reaction. Moreover, the energy band difference between guest and host will enhance the charge transfer between them.[31, 40] Apart from the high surface area and enhanced electron transfer efficiency, the large sized 2D nanosheets which constitute the layered NHs can act as an ideal optical scatter[41] as well. In this regard, the layered titania NHs are expected to be promising photoanode candidates, playing a tri-functional role (light harvesting, dye-adsorption and electron transfer) for high-efficiency DSSCs.

Scheme 1. Idealized Schematic Diagram of Photoanodes based on Layered NHs for Light Scattering.

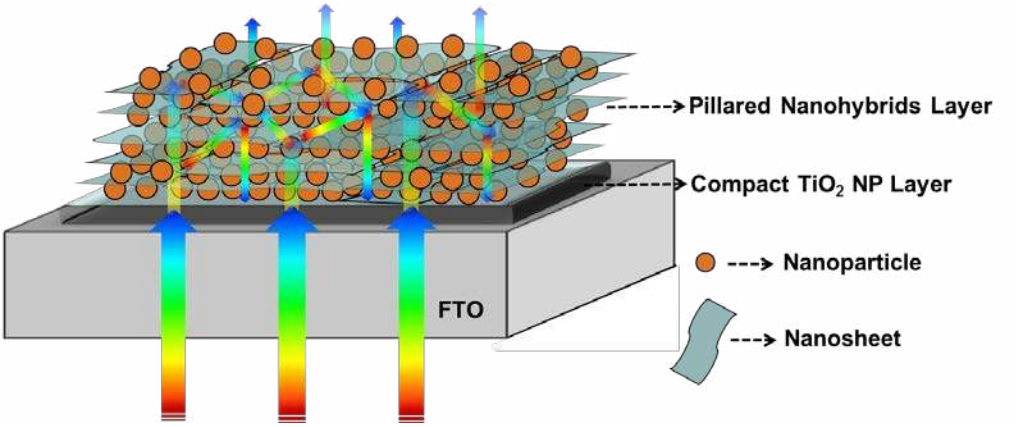

In this work, we report the layered NHs prepared by hybridizing the exfoliated titanate nanosheets ($Ti_{0.91}O_2$) with the anatase TiO_2 nanoparticles as shown in S-Figure. 1 for use as photoanodes in DSSCs. Our key strategy is to use exfoliation-reassembly strategy to introduce TiO_2 nanoparticles ranging from 7 to 9 nm (S-Figure. 2b) into the interlayers of 2D exfoliated $Ti_{0.91}O_2$ nanosheets (S-Figure. 2a) without deterioration of their fundamental crystal structures. In this way, the porosity and surface area of the NHs are expected to be significantly enlarged which is beneficial for sufficient dye-adsorption, and sub-micrometer sized nanosheets like the light shield will play a vital role in increasing the light scattering as shown in the idealized Scheme 1. In addition, we hypothesize the electron-hole recombination would be effectively suppressed due to the charge transfer between the guest and host in the layered NH system.[22, 23, 31] An enhanced overall conversion efficiency of 10.1% for layered titania nanosheet/ nanoparticle hybrid photoanode was achieved, a noticeable 29.5% improvement compared with the photoelectrode made of the benchmark Degussa TiO_2 P25 under the same testing conditions. Various characterizations confirmed our hypothesis and the feasibility of using new layered NH photoanodes for efficiency improvement of DSSCs.

EXPERIMENTAL SECTION

Preparation of Titania Nanosheet/ Nanoparticle Nanohybrids. Titania nanosheet ($Ti_{0.91}O_2$) suspension was prepared according to Sasaki's method.[35, 36, 42, 43] Layered titanate precursor $Cs_{0.68}Ti_{1.83}O_4$ was first prepared via a solid state reaction. In a typical synthesis, Cs_2CO_3 (7.694 g) and TiO_2 (10.0 g) powders were ground for at least half an hour to obtain adequately mixture. The mixture was transferred to an alumina crucible and calcined at 760 ℃ for 30 minutes. The mixed powder was then re-ground for half an hour and re-calcined at 760 ℃ for 12 hours. The obtained $Cs_{0.68}Ti_{1.83}O_4$ powder was subsequently proton-exchanged with excess amount of HCl (1M) for 3 days, and the HCl solution was refreshed every 24 hours. The protonated titanate precursor $H_{0.68}Ti_{1.83}O_4 \cdot H_2O$ was dispersed in tetrabutylammonium hydroxide (TBAOH) solution containing the same amount of protons intercalated in the layered titanate. The white suspension was then shaken for over 1 week. To remove the un-exfoliated titanates, the suspension was centrifuged under 4700 rpm for 5min and the supernatant suspension was collected for use. The obtained $Ti_{0.91}O_2$ Titania nanosheets suspension has a concentration of around 1.79 g/ L.

Anatase nanoparticles were prepared via a hydrolysis method. In a typical preparation process, 1-propanol (19.9ml) and titanium isopropoxide (43.8ml) were first mixed. The mixed solution was then dropwise added to 300ml of diluted HNO_3 solution (0.055M) under vigorous stirring, and a white suspension can be observed. The white suspension was kept at 70~80 ℃ in water bath for 8 hours until opaque white suspension was obtained. Thereafter, the opaque white suspension was ultrasonicated by ultrasonication probe for 30 minutes. The anatase nanoparticles suspension had a concentration of 0.407M. To prepare the anatase nanoparticle paste, diluted ammonia solution was added dropwise to the suspension under stirring until precipitates appeared. The top clear water was removed after standing for several hours and then the precipitates were dried at 50 ℃.

Titania NHs between nanosheets and anatase nanoparticles were synthesized as follows: under vigorous stirring, anatase nanoparticle suspension (8.8 ml) was added to nanosheet suspension (40 ml) dropwise. The suspension was then kept under 60 ℃ overnight. To obtain the nanohybrids, the suspension was centrifuged and washed with distilled water and ethanol for several times.

Preparation of TiO_2 Photoanodes. To prepare the DSSC photoanodes, FTO substrates (2.2 mm thickness, 8 Ω/ sq, Dyesol Glass) was cleaned with 2-propanol in an ultrasonic bath for 30 min, followed by thoroughly rinsing with water. A compact layer (ca. 110 nm) was firstly prepared by dip-coating TiO_2 organic sol[44] on the cleaned FTO surface, which not only have blocking effect but also can improve adherence between the TiO_2 layer and FTO substrates. As described in our previous work[45], TiO_2 pastes of various samples including P25, anatase nanoparticle (NP) and layered titania nanohybrids (NHs) were prepared and then deposited on the FTO glass pre-treated with a TiO_2 organic sol[44] by the doctor-blade method[45], and kept in a clean box for at least 15 min before heat treatment to reduce the surface irregularity and mechanical stress of the pastes. The working electrodes were put into a muffle furnace and heated at 450 ℃ for 30 min. Finally, all the films were post-treated again with TiO_2 organic sol.

Characterization of Layered NHs Powder and Films. The crystalline phase and structure of the samples were determined by using a Bruker Advanced X-Ray Diffractometer (40 kV, 30 mA) with Cu $K\alpha_1$ (λ=0.15406 nm) radiation. The morphology of the

layered NHs powder and films were examined by transmission electron microscopy (TEM, Tecnai Field Emission F20) and scanning electron microscopy (SEM, JEOL 6300). Brunauer-Emmett-Teller (BET) surface areas (S_{BET}) were analyzed with nitrogen

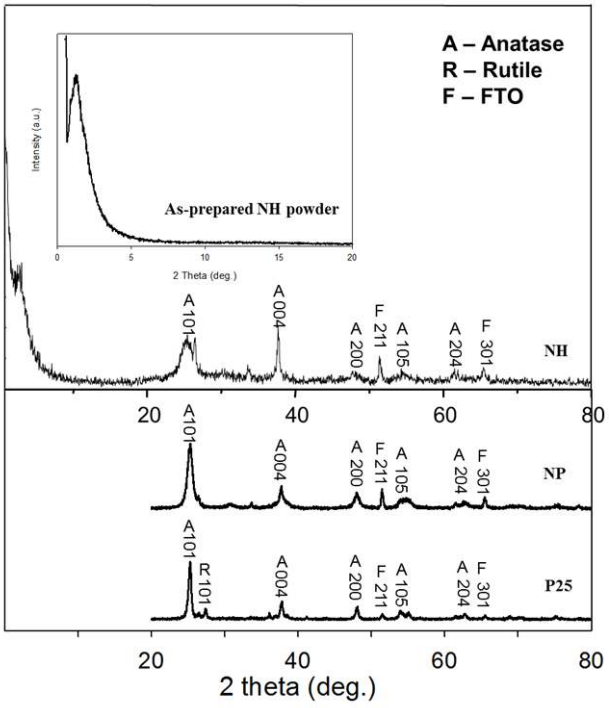

Figure 1. XRD patterns of P25, TiO_2 nanoparticle (NP), layered titania nanohybrid (NH) films on FTO substrates and as-prepared layered titania NHs powder.

adsorption apparatus (Quadrasorb SI). The film powder was obtained by scratching calcined films off FTO glass and all samples were degassed at 200 °C overnight before the measurement. The dye desorption was performed by immersing the dye-sensitized films in a 0.1M of NaOH in ethanol-water (v/v=1:1) solution[9]. The dye-uptake capacity of each photoanode was determined from the absorption value for each NaOH/dye solution by UV-vis spectrophotometer (Shimadzu UV-2450). The scattering and absorption properties of all samples were investigated with UV-visible diffused reflectance/light absorption spectrometer (Shimadzu UV-2450).

Fabrication and Measurements of DSSCs. Dye-loading was performed by immersing the working electrodes into a 0.5 mM N719 (Dyesol) dye solution in a 1:1 (v/v) mixture of acetonitrile and tert-butanol, and kept for 12-14 hours. Counter electrodes were fabricated by spin-coating H_2PtCl_6 isopropanol solution (5mM) on FTO substrates and heating at 380 °C for 15 min.[44] Then the dye-sensitized working electrode and Pt-counter electrode were assembled into a sandwich-type cell as described in our previous work.[46]

The photocurrent density-voltage (J-V) curves were recorded by using an Oriel AM 1.5 solar simulator equipped with an AM 1.5G type filter (Newport, 81094) and a Keithley model 2420 digital source meter. The dark current scan was performed in the similar condition but without illumination. IPCE plotted as a function of excitation wavelength was obtained by using a Newport 1918-c power meter under the irradiation of a 300 W Oriel xenon light source with an Oriel Cornerstone 260 1/4 m monochromator in DC mode.[14] The open-circuit voltage decay (OCVD) was carried out by switching off the illumination on DSSC on a steady state and

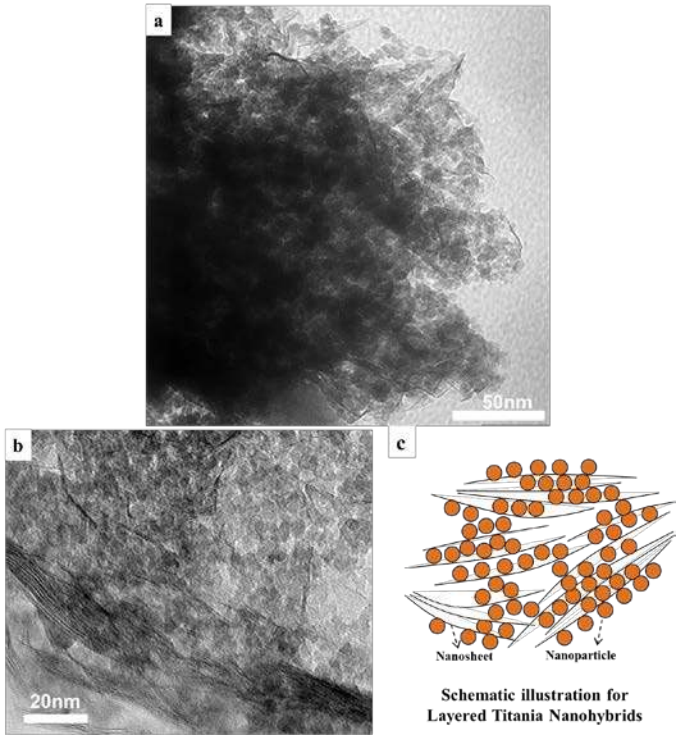

Figure 2. (a) Typical TEM image of the restacked NH sample; (b) high-magnification TEM image showing the lamellar structure; (c) schematic illustration of layered titania NHs.

monitoring the decay of the open-circuit voltage (V_{oc}).[20] Electrochemical impedance spectroscopy (EIS) was mearsured by the Solartron 1480 Potentiostat in a frequency range of 10^6 - 0.1 Hz under dark and the applied bias voltage and ac amplitude were set as -0.7 V and 10 mV.[14]

RESULTS AND DISCUSSION

Characterization of Layered NH powder and Various Films

The resultant layered NH powder and various films were comprehensively characterized and Figure 1 shows XRD patterns of the as-prepared NH powder and films prepared with P25, sol-gel derived TiO_2 nanoparticles (NP) and NH samples printed on FTO substrates. As indicated in the XRD patterns, both the NP and NH samples are pure anatase (A) phase (JCPDS No. 21-1272) with typical peaks (101), (004) and (200), whereas all diffraction peaks of the P25 films can be well indexed to a mixture of anatase (A) TiO_2, and rutile (R) TiO_2 (JCPDS No. 21-1276). Peaks F belong to FTO substrates. The Raman spectrum of NH film further confirmed the anatase phase with typical vibrational bands as marked on S-Figure 4. The inset shows a poorly-resolved 001 indice (2θ= 1.24°) for the as-prepared NH, which can be attributed to the formation of disordered porous titania heterostructure consisting of nanosheets and nanoparticles in some domains. An electrostatic interaction between negatively charged titanate nanosheets and positively charged TiO_2 nanoparticles is believed to be a driving force for the formation of such type disordered heterostructure.[22] The discernible broad 001 reflection for the NH film after heat treatment shifted toward the higher angle side (2θ= 2.46 °), indicative of the shrinkage in basal spacing mainly attributed to the dehydroxylation of TiO_2 nanosol particles but maintenance of the NH structure.

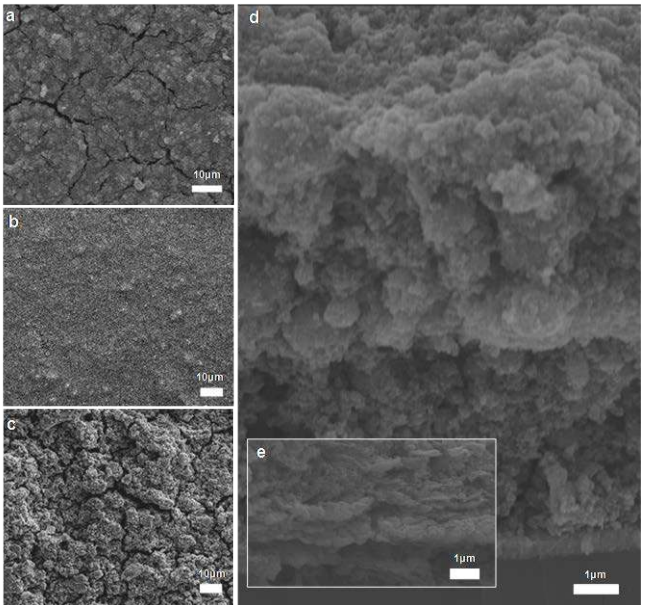

Figure 3. Surface SEM images of a) layered NH, b) P25 and c) nanoparticle films; d) cross-sectional SEM images of a whole layered NH film; e) high-magnification cross-sectional SEM images of randomly selected area in the layered NH film showing the layered structure.

The formation of the layered NH structure was further confirmed using TEM analysis. Figure 2a and S-Figure 3 depict the typical TEM image of restacked NHs. High-resolution TEM image in Figure 2b exhibits an assembly of parallel dark lines ($Ti_{0.91}O_2$ nanosheets) and spherical shapes (TiO_2 nanoparticles) in some domains. Unlike highly ordered pillared structure prepared from the restacking of exfoliated nanosheets with small-sized guest species such as Li^+, Al_{13}^+ clusters,[47, 48] it's understandable that restacking of larger TiO_2 nanoparticles with extremely thin nanosheets is much more difficult to control, thus leading to poorly-ordered layered structure. As shown in Figure 2a and b, the exfoliated $Ti_{0.91}O_2$ nanosheets are randomly hybridized with TiO_2 nanoparticles, which is in good agreement with the XRD results. Figure 2c is the idealized schematic illustration of the highly disordered NH structure for better understanding.

In order to further verify the disordered layered structure in the calcined films, SEM characterization was carried out to observe the resultant structures. The plate-like surface of NH film (Figure 3a) is quite different from that of P25 and NP films (Figure 3b, c). Although some micro-cracks can be found in SEM images, to some extent this can be optimized by a following post-treatment step with TiO_2 sol. The optical property (will be discussed later) also confirm that the light harvesting of the films was not affected much by such micro-cracks. As shown in the cross-sectional image (Figure 3d), all the films have a thickness of *ca*12.3 μm. High magnification cross-sectional images were taken randomly through the whole cross-section of the NH films. Upon heat treatment, disordered micron thick layer will be formed, consisting of several layers of nanosheets and nanoparticles. As shown in Figure 3e, the micron thick layered structure can be clearly visualized within the NH film after calcination.

The nitrogen adsorption-desorption isotherms of as-prepared NH powder and film powder scratched off from the calcined NH films shown in Figure 4 provide further evidence for the

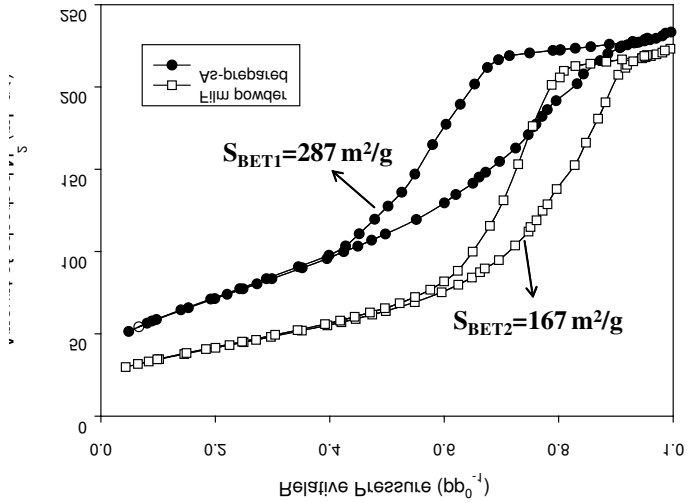

Figure 4. Nitrogen adsorption-desorption isotherms of as-prepared layered NHs powder and powder scratched off from the calcined NH films.

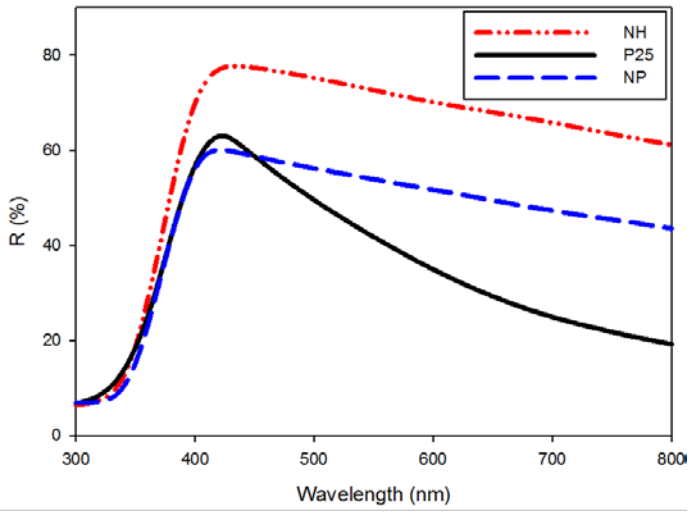

Figure 5. Diffused reflectance spectra of the P25, NP and layered NH films.

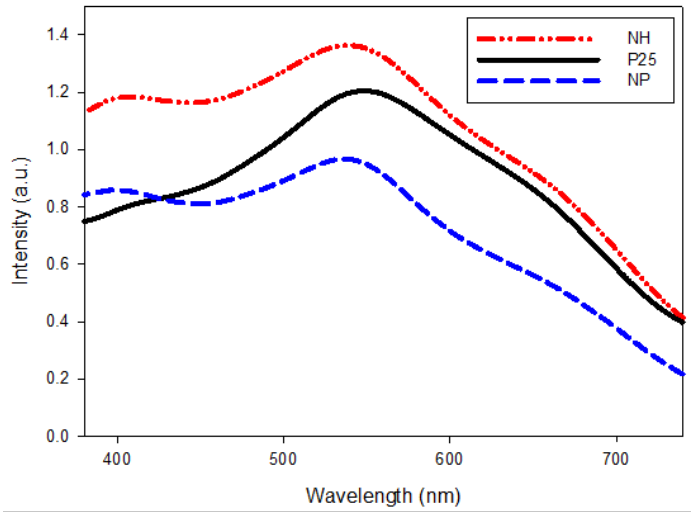

Figure 6. UV-vis absorption spectra of the P25, NP and layered NH films with dye adsorbed.

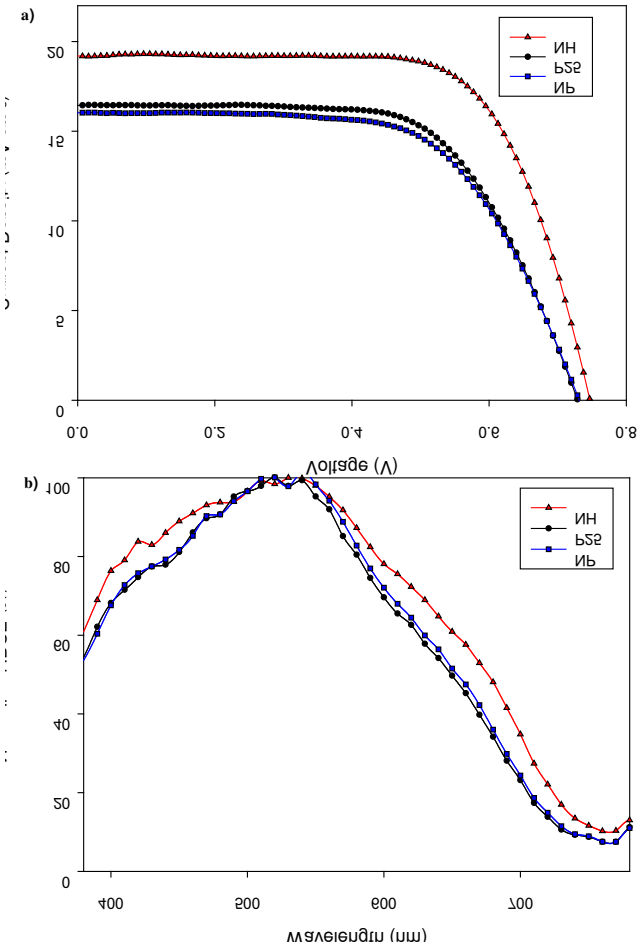

Figure 7. a) *J-V* curves and b) Normalized IPCE of DSSCs based on P25, NP and layered NH photoanodes.

formation of porous layered structure by reassembling exfoliated $Ti_{0.91}O_2$ nanosheets in the presence of anatase nanoparticles. The NHs shows a type IV isotherm, characteristics of mesoporous structure in the materials. This clearly reveals that the mesopores in the NHs were developed by random hybridization of $Ti_{0.91}O_2$ nanosheets with anatase nanoparticles. In addition, the mesoporous NHs show the type H3 hysteresis loop in the IUPAC classification, suggesting that the slit-shaped pores were formed. As shown in Figure 4, the Brunauer-Emmett-Teller (BET) specific surface area of the as-prepared samples was quite high (287 m^2/g), the film powder decreased to 167 m^2/g as a result of heat treatment at 450 °C.

Diffused Reflectivity and UV-vis Absorption

The reflectivity of each film was studied to investigate the scattering effect of the layered NHs. Figure 5 shows the diffused reflectance spectra of various samples. Apparently, layered NH films had much higher reflectivity in the wavelength range of 380~800 nm than that of NP and P25 films. This evidence confirms our hypothesis on the efficient light scattering of layered NHs acting as light shields. Note that the reflectivity of NP film is slightly higher than that of P25 film in the same wavelength range, possibly due to the aggregation of sol-gel prepared nanoparticles (Figure 3c). In order to study the photovoltaic properties of DSSCs based on the layered NHs, dye- loading was first investigated (Table 1). Prior to dye-loading measurement, UV-vis absorption

Table 1. Comparison of Photovoltaic Properties, BET Surface Area and Dye-loading of P25, NP and Layered NH Photoanodes.

Samples	J_{sc} [mA/cm^2]	V_{oc} [V]	*FF* [%]	η^a [%]	S_{BET} Value [m^2/g]	Dye-loading^b [10^{-7} mol/cm^2]
P25	16.4	0.73	65	7.8	51	1.80
NP	15.9	0.73	64	7.4	43	1.65
NH	19.2	0.75	70	10.1	167	2.05

[a] Measurements were performed under AM 1.5G one sun (light intensity: 100 $mWcm^{-2}$), the active areas were ca. 0.16 cm^2 for all of the cells and the average value of each data was obtained by testing 6~8 cells.
[b] Dye-absorbed films with a dimension of *ca.* 3 cm^2 were used for estimating the dye uptake.

was carried out for all three different films with dye adsorbed as shown in Figure 6. Compared with the TiO_2 nanoparticle films (NP and P25), the layered NH films showed a higher absorption in the wavelength range from 400 nm to 700 nm, which is consistent with the significantly increased dye-loading indicated in Table 1 and corresponding photos as shown in S-Figure 5. In addition, we found that as monolayer adsorption[49, 50] the dye-loading amount is quite comparable with those reported in other literatures.[7, 9, 17] This higher dye-loading can be attributed to the large surface area of the layered NH films, as verified by BET specific surface area (S_{BET}) measurements (Table 1).

Photocurrent Density-Voltage (J-V) Characteristics

The photovoltaic performance of layered NH photoelectrode were analyzed against the photoelectrodes fabricated with P25 and NP as listed in Table 1, with the short current density-voltage (*J-V*) characteristics of DSSCs shown in Figure 7a. Table 1 compares the photovoltaic properties of DSSCs based on various films with a thickness of *ca.* 12.3 μm. Due to insufficient light harvesting and inefficient electron transfer, DSSCs assembled with P25 showed a limited efficiency of 7.8% (comparable with the efficiency reported in literature[9, 12, 51] as well as that of devices made from Dyesol paste shown in S-Figure 7), with relatively small J_{sc} (16.4 mA cm^{-2}), open-circuit voltage (V_{oc}, 0.73V) and fill factor (FF, 65%). Whereas all the key parameters of DSSCs based on layered NHs were improved (J_{sc}: 19.2 mA cm^{-2}; V_{oc}: 0.75 V; *FF*: 70%), which resulted in enhanced overall conversion efficiency (η) of 10.1% (close to the champion efficiency of 12.3%[52]). The possible explanation for the higher V_{oc} of the hybrid cells is the blocking of recombination as a result of charge transfer[22, 23, 30, 31, 53, 54] within the layered NH film, which results in an increase in electron density in TiO_2, and thus the shift of Fermi level.[55] As evidenced above, the large surface area makes it accessible for more dye-adsorption, and the light scattering effect of the re-assembled exfoliated titanates favour enhanced light-harvesting efficiency by increasing the optical length serving as light-scattering shield, and thereby enhanced J_{sc} for the cell with the layered NH film.[5, 56] The faster electron diffusion rate[57, 58] in the NH film can be considered as the reason for the higher *FF* of the cell assembled with NH films, as compared with the cell using P25 film.

Note that the DSSC made of anatase nanoparticle (NP) film showed a slightly decreased J_{sc} and η. This could be mainly caused by the lower dye loading in this NP film due to the decreased surface area as a result of aggregation. Whereas in the case of layered NH sample, the randomly hybridized layered $Ti_{0.91}O_2$ inhibit TiO_2 nanoparticle growth upon calcination.

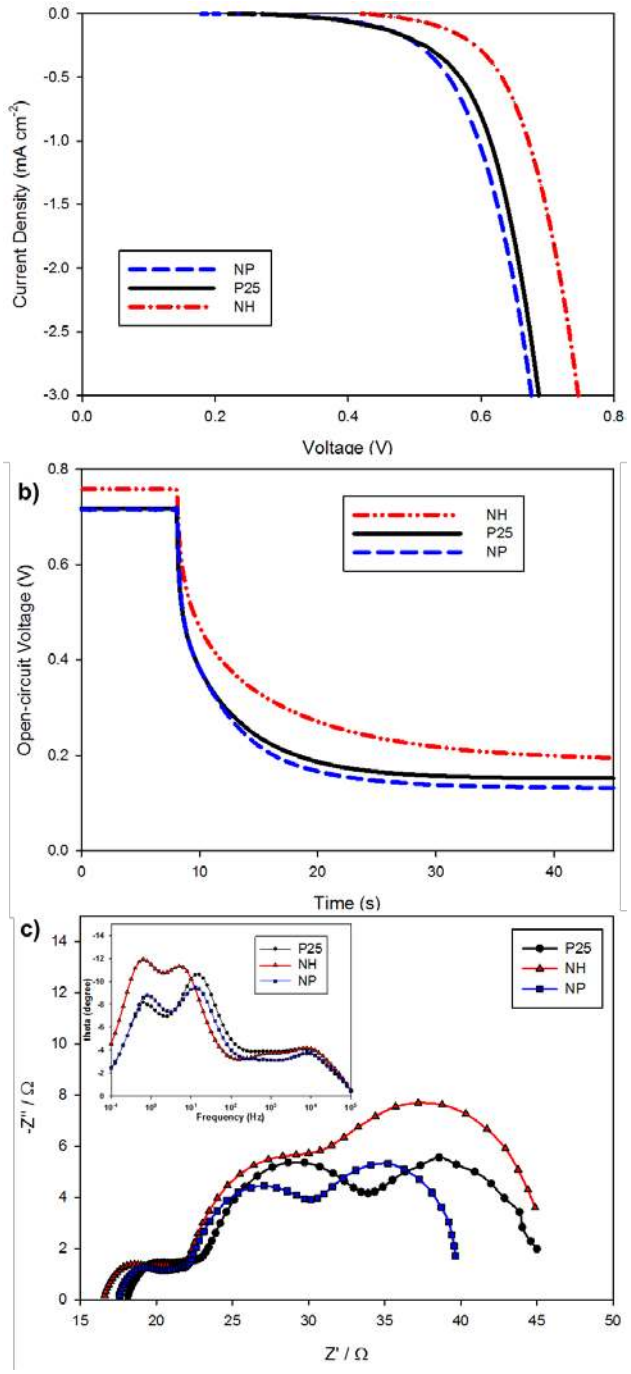

Figure 8. a) Dark current potential scans, b) Open-circuit voltage decay profiles and c) impedance spectra of DSSCs based on P25, NP and layered NH photoanodes. The Bode phase plot is shown in the inset of (c).

Incident Photon-to-Current Conversion Efficiency (IPCE) Performance

The IPCE spectra of the various photoanodes as a function of the illumination wavelength can provide further evidence on the scattering effect of the NH structure. The IPCE of the NH film based DSSCs (S-Figure 6) showed a considerable increase over the entire wavelength range. To better determine the superior optical characteristic of the titania nanohybrids, the normalized IPCE was obtained by normalizing the measured IPCE to the maximum intensity of 520nm, as shown in Figure 7b. We can then clearly visualize the impact of this new NH structure on the light conversion efficiency of the lower energy photons in the long wavelength range, from 560 nm until far in the absorption tail (up to 750 nm). The full spectrum enhancement of NH devices compared with that of P25 and NP should be evidently attributed to the increased dye-adsorption (large surface area) and efficient light scattering (nanosheets component).

Dark Current, OCVD and EIS

To further investigate the origin and evidence for the enhanced efficiency especially the improved V_{oc} and FF of the layered NH based cells, the dark current potential scans were performed as shown in Figure 8a, which was employed to estimate the charge carrier recombination in DSSCs. It is generally believed that electron recombination is attributed to the reduction of I_3^- ions by electrons on the FTO substrate, which will result in a decrease in photocurrent.[59] Compared with the NP and P25 film, the onset of dark current for DSSCs with the layered NH film occurred at a higher potential and a smaller dark current was produced under the same bias above 0.4 V. This result indicates a slower recombination rate between the transferred electrons and I_3^- ions for the NH film.[60, 61] Since the suppression of back electron transfer in the layered NHs, the increased V_{oc} and *FF* were achieved and consequently improved overall conversion efficiency.

The open-circuit voltage decay (OCVD) technique was employed to further examine the charge transfer kinetics of the DSSCs. Before the measurement, a steady-state voltage for the DSSC cell was obtained under illumination and the subsequent decay of V_{oc} was then recorded after the illumination was interrupted. The decay of the V_{oc} can be viewed as a sign of electron loss as a result of the electron-hole recombination.[20, 62] As shown in Figure 8b, the decay rate of V_{oc} is apparently slower in DSSCs assembled with the layered NHs, implying a reduced charge recombination rate in comparison with that of DSSCs fabricated by anatase NP and P25, which is in good agreement with the result in Figure 8a.

To better elucidate the electron transport and charge recombination in NH photoelectrodes, electrochemical impedance spectroscopy (EIS) was performed in the dark under a forward bias of -0.7 V as shown in Figure 8c and the inset shows the Bode phase plot. As observed in the Nyquist plots, the radius of the middle semicircle increase in the order NP ‹ P25 ‹ NH, implying a larger electron recombination resistance for NH electrodes.[63] In addition, the middle-frequency peak of DSSCs based on NH electrodes shown in the Bode phase plots shifts to lower frequency relative to P25 and NP, which indicates that the electron lifetime was prolonged in NH based DSSCs.[64] Therefore, the larger electron recombination resistance and longer electron lifetime observed in NH relative to P25 and NP based DSSCs illustrate more effective suppression of the back reaction of the injected electron with the I_3^- in the electrolyte due to the electron transfer between guest and host,[22, 23, 31] and better explained the observed improvements in both the photocurrent and photovoltage, yielding substantially enhanced energy conversion efficiency.[63]

CONCLUSIONS

In summary, a new type of porous layered titania NHs were successfully prepared by hybridizing the exfoliated titanate with the anatase TiO_2 nanosol, which was subsequently used as a trifunctional photoanode for high efficiency DSSCs. Reflectance spectra demonstrate that the light-harvesting efficiency of the NH films was significantly higher than that of P25 film due to the effective light-scattering of $Ti_{0.91}O_2$ nanosheets. The larger surface area of the layered NH films leading to increased dye-loading is veri-

fied by BET specific surface area measurements. In addition, not only the dark current potential scan but also the open circuit voltage decay indicates a lower charge recombination for photoelectrode fabricated with NHs. The DSSCs assembled using photoanode with layered NHs demonstrated a high overall conversion efficiency of 10.1%, remarkably enhanced by 29.5% compared to that (7.8%) obtained from the benchmark P25 nanoparticles. Layered NHs may lead to a new way in the fine-tuning of photoanode structures for high efficiency DSSCs as well as boosting the efficiency of Quantum dot-sensitized solar cells.

ASSOCIATED CONTENT

Supplementary figures. This material is available free of charge via the Internet at http://pubs.acs.org.

AUTHOR INFORMATION

Corresponding Author

*Email: l.wang@uq.edu.au

Notes

The authors declare no competing financial interest.

ACKNOWLEDGMENT

This work was financially supported by the Australian Research Council (ARC) through Discovery Projects. YB acknowledges the support from Chinese Scholarship Council (CSC).

REFERENCES

1. O'Regan, B.; Gratzel, M., *Nature* **1991,** 353, 6346, 737-740.
2. Ko, S. H.; Lee, D.; Kang, H. W.; Nam, K. H.; Yeo, J. Y.; Hong, S. J.; Grigoropoulos, C. P.; Sung, H. J., *Nano Lett.* **2011,** 11, 2, 666-671.
3. Liu, B.; Aydil, E. S., *J Am. Chem. Soc.* **2009,** 131, 11, 3985-3990.
4. Zhang, Q. F.; Chou, T. P.; Russo, B.; Jenekhe, S. A.; Cao, G. Z., *Angew. Chem. Int. Ed.* **2008,** 47, 2402-6.
5. Law, M.; Greene, L. E.; Johnson, J. C.; Saykally, R.; Yang, P., *Nat. Mater.* **2005,** 4, 6, 455-459.
6. Zhu, K.; Neale, N. R.; Miedaner, A.; Frank, A. J., *Nano Lett.* **2007,** 7, 1, 69-74.
7. Huang, F. Z.; Chen, D. H.; Zhang, X. L.; Caruso, R. A.; Cheng, Y. B., *Adv. Funct. Mater.* **2010,** 20, 8, 1301-1305.
8. Yan, K. Y.; Qiu, Y. C.; Chen, W.; Zhang, M.; Yang, S. H., *Energy Environ. Sci.* **2011,** 4, 6, 2168-2176.
9. Wu, X.; Lu, G. Q.; Wang, L., *Energy Environ. Sci.* **2011,** 4, 9, 3565-3572.
10. Koo, H. J.; Kim, Y. J.; Lee, Y. H.; Lee, W. I.; Kim, K.; Park, N. G., *Adv. Mater.* **2008,** 20, 1, 195-199.
11. Qian, J. F.; Liu, P.; Xiao, Y.; Jiang, Y.; Cao, Y. L.; Ai, X. P.; Yang, H. X., *Adv. Mater.* **2009,** 21, 36, 3663-3667.
12. Yu, H.; Bai, Y.; Zong, X.; Tang, F. Q.; Lu, G. Q. M.; Wang, L. Z., *Chem. Commun.* **2012,** 48, 59, 7386-7388.
13. Zhang, H. M.; Han, Y. H.; Liu, X. L.; Liu, P.; Yu, H.; Zhang, S. Q.; Yao, X. D.; Zhao, H. J., *Chem. Commun.* **2010,** 46, 44, 8395-8397.
14. Bai, Y.; Yu, H.; Li, Z.; Amal, R.; Lu, G. Q.; Wang, L. Z., *Adv. Mater.* **2012,** 24, 43, 5850-5856.
15. Ohsaki, Y.; Masaki, N.; Kitamura, T.; Wada, Y.; Okamoto, T.; Sekino, T.; Niihara, K.; Yanagida, S., *Phys. Chem. Chem. Phys.* **2005,** 7, 24, 4157-4163.
16. Zhu, K.; Vinzant, T. B.; Neale, N. R.; Frank, A. J., *Nano Lett.* **2007,** 7, 12, 3739-3746.
17. Adachi, M.; Murata, Y.; Takao, J.; Ju, J. T.; Sakamoto, M.; Wang, F. M., *J Am. Chem. Soc.* **2004,** 126, 45, 14943-14949.
18. Xu, F.; Sun, L., *Energy Environ. Sci.* **2011,** 4, 3, 818-841.
19. Lin, C. Y.; Lai, Y. H.; Chen, H. W.; Chen, J. G.; Kung, C. W.; Vittal, R.; Ho, K. C., *Energy Environ. Sci.* **2011,** 4, 9, 3448-3455.
20. Wu, X.; Chen, Z. G.; Lu, G. Q.; Wang, L. Z., *Adv. Funct. Mater.* **2011,** 21, 21, 4167-4172.
21. Fujishiro, Y.; Uchida, S.; Sato, T., *Int. J. Inorg. Mater.* **1999,** 1, 1, 67-72.
22. Kim, T. W.; Hur, S. G.; Hwang, S. J.; Park, H.; Choi, W.; Choy, J. H., *Adv. Funct. Mater.* **2007,** 17, 2, 307-314.
23. Choy, J. H.; Lee, H. C.; Jung, H.; Kim, H.; Boo, H., *Chem. Mater.* **2002,** 14, 6, 2486-2491.
24. Geng, F.; Ma, R.; Nakamura, A.; Akatsuka, K.; Ebina, Y.; Yamauchi, Y.; Miyamoto, N.; Tateyama, Y.; Sasaki, T., *Nat Commun* **2013,** 4, 1632.
25. Paek, S.-M.; Jung, H.; Park, M.; Lee, J.-K.; Choy, J.-H., *Chem. Mater.* **2005,** 17, 13, 3492-3498.
26. Shibata, T.; Takanashi, G.; Nakamura, T.; Fukuda, K.; Ebina, Y.; Sasaki, T., *Energy Environ. Sci.* **2011,** 4, 2, 535-542.
27. Ko, J.; Kim, I.; Hwang, S.; Jung, H., *J Nanosci. Nanotechnol.* **2011,** 11, 2, 1726.
28. Xu, B.-H.; Lin, B.-Z.; Wang, Q.-Q.; Pian, X.-T.; Zhang, O.; Fu, L.-M., *Microporous Mesoporous Mater.* **2012,** 147, 1, 79-85.
29. Lin, B.; He, L.; Zhu, B.; Chen, Y.; Gao, B., *Catal. Commun.* **2012,** 29, 0, 166-169.
30. Lin, B.-Z.; Li, X.-L.; Xu, B.-H.; Chen, Y.-L.; Gao, B.-F.; Fan, X.-R., *Microporous Mesoporous Mater.* **2012,** 155, 0, 16-23.
31. Yanagisawa, M.; Uchida, S.; Fujishiro, Y.; Sato, T., *J Mater. Chem.* **1998,** 8, 12, 2835-2838.
32. Liu, G.; Wang, L.; Yang, H. G.; Cheng, H.-M.; Lu, G. Q., *J Mater. Chem.* **2010,** 20, 5, 831-843.
33. Akatsuka, K.; Takanashi, G.; Ebina, Y.; Haga, M.-a.; Sasaki, T., *J Phys. Chem. C* **2012,** 116, 23, 12426-12433.
34. Osada, M.; Sasaki, T., *ECS Trans.* **2013,** 50, 6, 111-116.
35. Sasaki, T.; Watanabe, M.; Hashizume, H.; Yamada, H.; Nakazawa, H., *J Am. Chem. Soc.* **1996,** 118, 35, 8329-8335.
36. Sasaki, T.; Watanabe, M., *J Am. Chem. Soc.* **1998,** 120, 19, 4682-4689.
37. Paek, S. M.; Jung, H.; Lee, Y. J.; Park, M.; Hwang, S. J.; Choy, J. H., *Chem. Mater.* **2006,** 18, 5, 1134-1140.
38. Kim, T. W.; Ha, H. W.; Paek, M. J.; Hyun, S. H.; Baek, I. H.; Choy, J. H.; Hwang, S. J., *J Phys. Chem. C* **2008,** 112, 38, 14853-14862.
39. Kim, T. W.; Hwang, S. J.; Jhung, S. H.; Chang, J. S.; Park, H.; Choi, W.; Choy, J. H., *Adv. Mater.* **2008,** 20, 3, 539-542.
40. Choy, J. H.; Lee, H. C.; Jung, H.; Kim, H.; Boo, H., *Chemistry of Materials* **2002,** 14, 6, 2486-2491.
41. Qiu, Y. C.; Chen, W.; Yang, S. H., *J Mater. Chem.* **2010,** 20, 5, 1001-1006.
42. Sasaki, T.; Ebina, Y.; Kitami, Y.; Watanabe, M.; Oikawa, T., *J Phys. Chem. B* **2001,** 105, 26, 6116-6121.
43. Liu, G.; Wang, L. Z.; Sun, C. H.; Chen, Z. G.; Yan, X. X.; Cheng, L. N.; Cheng, H. M.; Lu, G. Q., *Chem. Commun.* **2009,** 0, 11, 1383-1385.
44. Yu, H.; Zhang, S. Q.; Zhao, H. J.; Will, G.; Liu, P., *Electrochim. Acta* **2009,** 54, 4, 1319-1324.

45. Mills, A.; Elliott, N.; Hill, G.; Fallis, D.; Durrant, J. R.; Willis, R. L., *Photochem. Photobiol. Sci.* **2003,** 2, 5, 591-596.
46. Ito, S.; Murakami, T. N.; Comte, P.; Liska, P.; Grätzel, C.; Nazeeruddin, M. K.; Grätzel, M., *Thin Solid Films* **2008,** 516, 14, 4613-4619.
47. Wang, L. Z.; Sakai, N.; Ebina, Y.; Takada, K.; Sasaki, T., *Chem. Mater.* **2005,** 17, 6, 1352-1357.
48. Wang, L. Z.; Omomo, Y.; Sakai, N.; Fukuda, K.; Nakai, I.; Ebina, Y.; Takada, K.; Watanabe, M.; Sasaki, T., *Chem. Mater.* **2003,** 15, 15, 2873-2878.
49. Grätzel, M., *J. Photochem. Photobiol., A* **2004,** 164, 1–3, 3-14.
50. Harms, H. A.; Tetreault, N.; Gusak, V.; Kasemo, B.; Gratzel, M., *Phys. Chem. Chem. Phys.* **2012,** 14, 25, 9037-9040.
51. Zhang, H.; Han, Y.; Liu, X.; Liu, P.; Yu, H.; Zhang, S.; Yao, X.; Zhao, H., *Chem. Commun.* **2010,** 46, 44, 8395-8397.
52. Yella, A.; Lee, H.-W.; Tsao, H. N.; Yi, C.; Chandiran, A. K.; Nazeeruddin, M. K.; Diau, E. W.-G.; Yeh, C.-Y.; Zakeeruddin, S. M.; Grätzel, M., *Science* **2011,** 334, 6056, 629-634.
53. Choy, J.-H.; Lee, H.-C.; Jung, H.; Hwang, S.-J., *J. Mater. Chem.* **2001,** 11, 9, 2232-2234.
54. Gunjakar, J. L.; Kim, I. Y.; Lee, J. M.; Lee, N.-S.; Hwang, S.-J., *Energy Environ. Sci.* **2013,** 6, 3, 1008-1017.
55. Tan, B.; Wu, Y. Y., *J. Phys. Chem. B* **2006,** 110, 32, 15932-15938.
56. Zhang, Q. F.; Dandeneau, C. S.; Zhou, X. Y.; Cao, G. Z., *Adv. Mater.* **2009,** 21, 41, 4087-4108.
57. Pang, S.; Xie, T. F.; Zhang, Y.; Wei, X.; Yang, M.; Wang, D. J.; Du, Z. L., *J. Phys. Chem. C* **2007,** 111, 49, 18417-18422.
58. Du, A. J.; Ng, Y. H.; Bell, N. J.; Zhu, Z. H.; Amal, R.; Smith, S. C., *J. Phys. Chem. Lett.* **2011,** *2*, 8, 894-899.
59. Ito, S.; Liska, P.; Comte, P.; Charvet, R.; Pechy, P.; Bach, U.; Schmidt-Mende, L.; Zakeeruddin, S. M.; Kay, A.; Nazeeruddin, M. K.; Gratzel, M., *Chem. Commun.* **2005**, 34, 4351-4353.
60. Huang, S. Y.; Schlichthorl, G.; Nozik, A. J.; Gratzel, M.; Frank, A. J., *J. Phys. Chem. B* **1997,** 101, 14, 2576-2582.
61. Gregg, B. A.; Pichot, F.; Ferrere, S.; Fields, C. L., *J. Phys. Chem. B* **2001,** 105, 7, 1422-1429.
62. Zaban, A.; Greenshtein, M.; Bisquert, J., *ChemPhysChem* **2003,** 4, 8, 859-864.
63. Kuang, D.; Uchida, S.; Humphry-Baker, R.; Zakeeruddin, S. M.; Grätzel, M., *Angew. Chem. Int. Ed.* **2008,** 47, 10, 1923-1927.
64. Liao, J.-Y.; Lin, H.-P.; Chen, H.-Y.; Kuang, D.-B.; Su, C.-Y., *J. Mater. Chem.* **2012,** 22, 4, 1627-1633.

Table of Contents

Supporting Information

Porous Titania Nanosheet/Nanoparticle Hybrids as Photoanodes for Dye-sensitized Solar Cells

Yang Bai,[a] Zheng Xing,[a] Hua Yu,[a] Zhen Li,[b] Rose Amal,[a] and Lianzhou Wang*[a]

[a]ARC Centre of Excellence for Functional Nanomaterials, School of Chemical Engineering and Australian Institute for Bioengineering and Nanotechnology, The University of Queensland, St Lucia, Brisbane, QLD 4072 Australia.

[b] Institute of Superconducting and Elctronic Materials, Australian Institute of Innovative Materials, The University of Wollongong, Squires Way, Northwollongong, NSW 2500, Australia.

[c]ARC Centre of Excellence for Functional Nanomaterials, School of Chemical Engineering, The University of New South Wales, Sydney, NSW, 2052, Australia.

*Corresponding Author. Email Address: l.wang@uq.edu.au

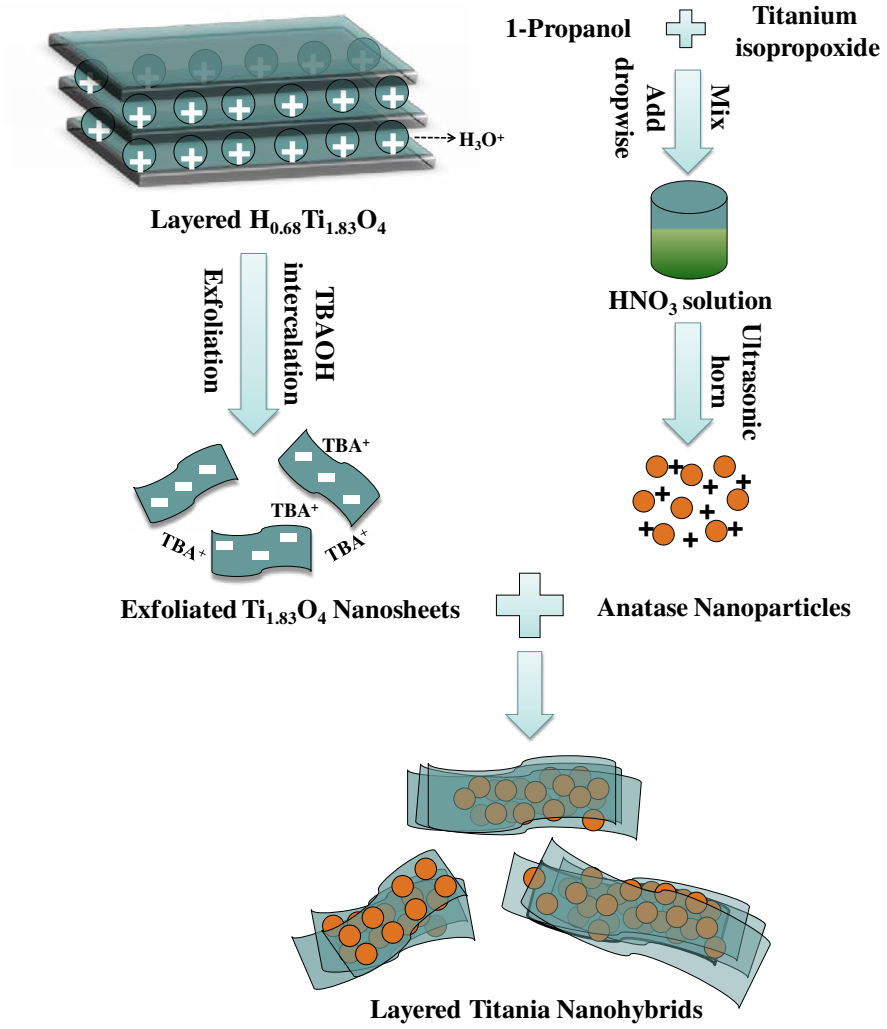

S-Figure 1 Schematic diagram for an exfoliation–hybridization route to prepare layered titania NHs

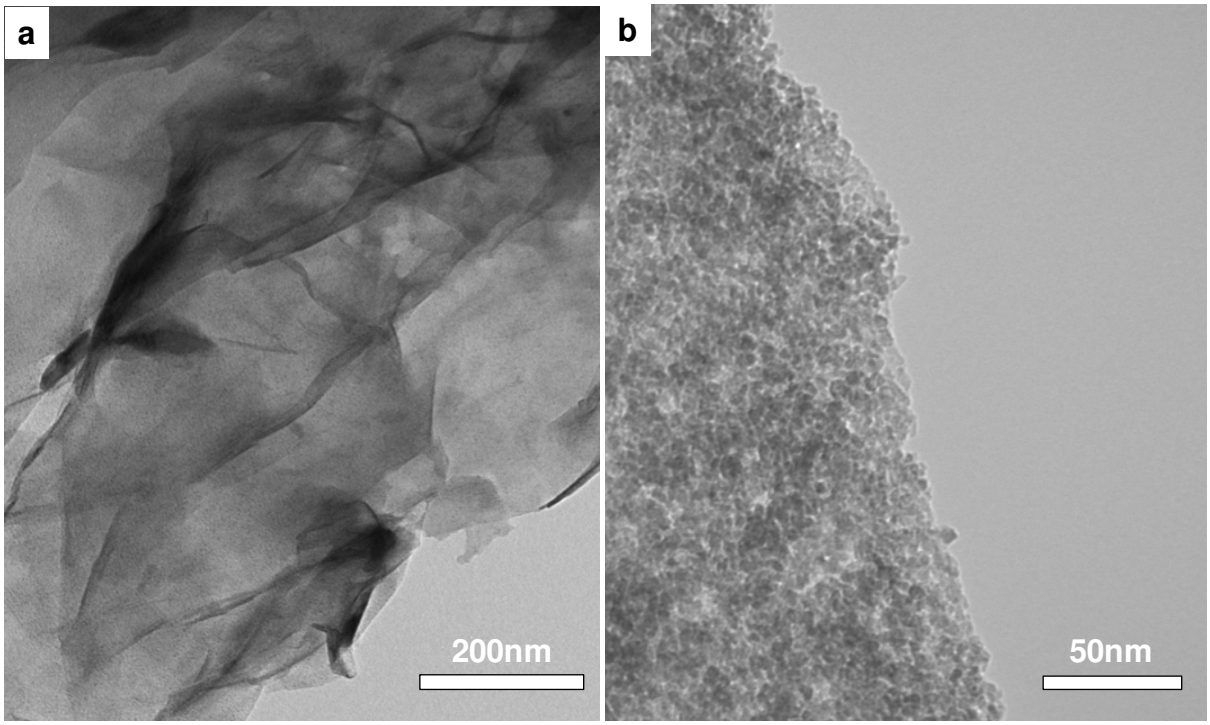

S-Figure 2 TEM of a) exfoliated $Ti_{0.91}O_2$ nanosheets, and b) anatase nanoparticle prepared from hydrolysis of titanium isopropoxide.

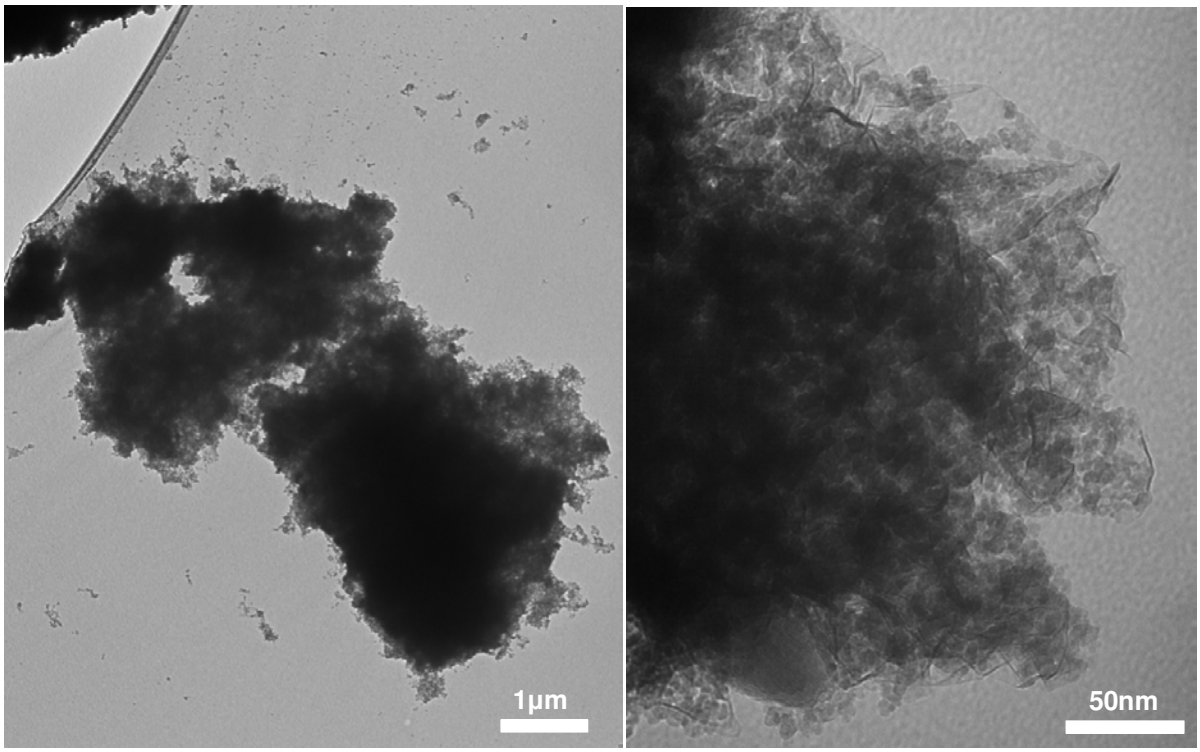

S-Figure 3 TEM of restacked nanohybrids.

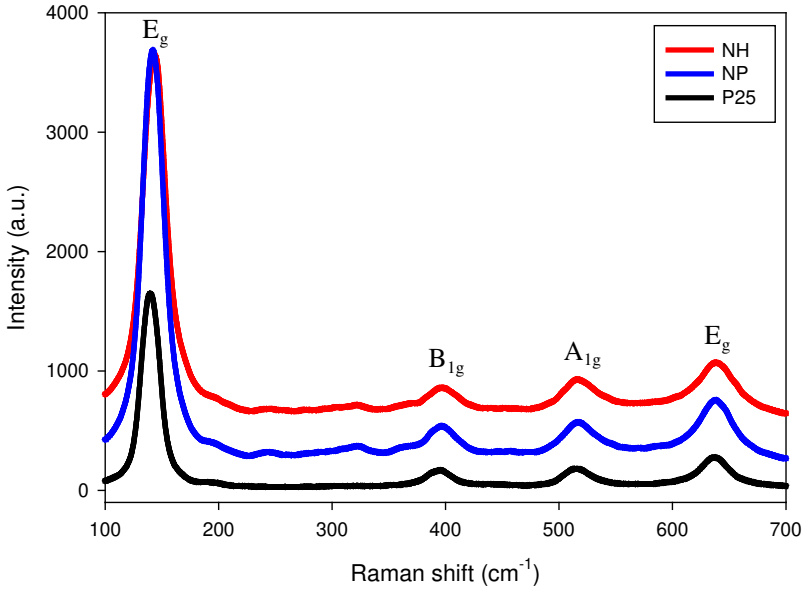

S-Figure 4 Raman spectra of P25, NP and NH films.

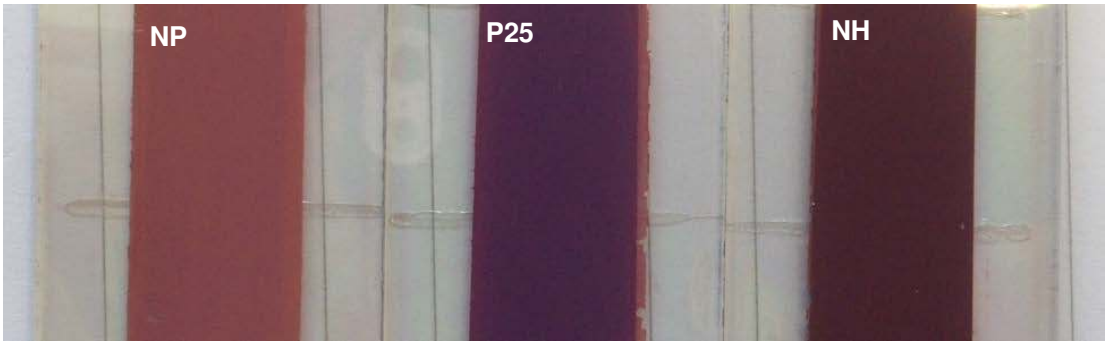

S-Figure 5 Corresponding photos of NP, P25 and NH films after dye adsorption.

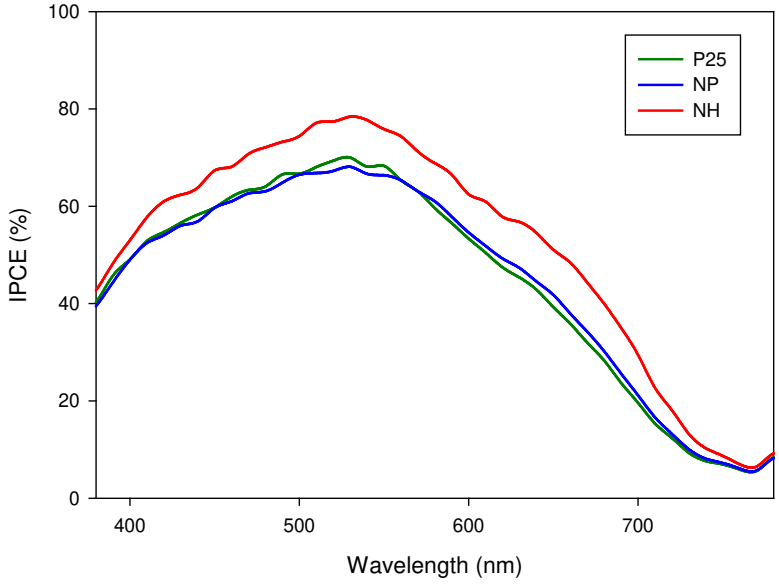

S-Figure 6 IPCE of DSSCs based on P25, NP and NH photoanodes.

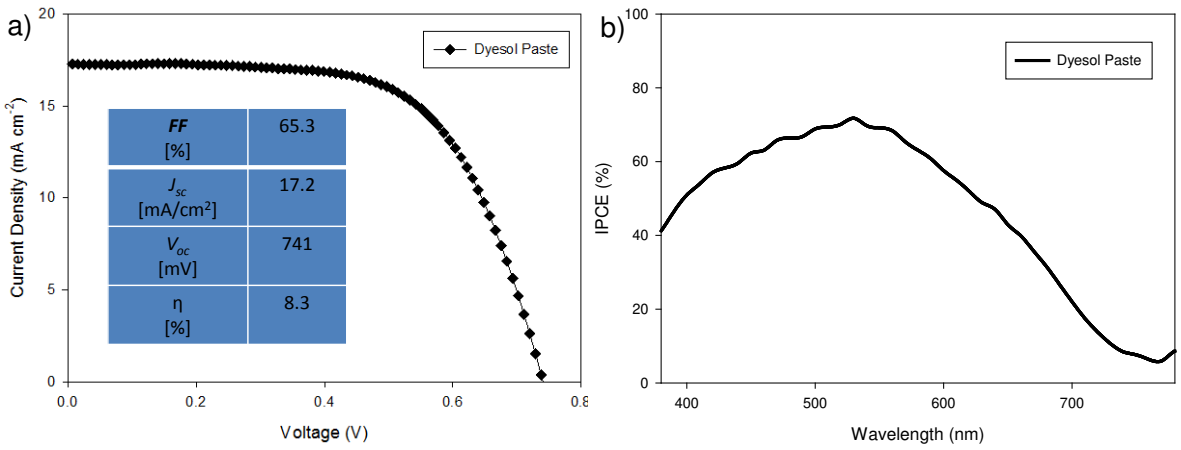

S-Figure 7 a) *J-V* curves and b) IPCE of DSSCs based on photoanodes composed of commercial Dyesol paste (18NR-T Transparent Titania Paste).